Journal of the Korean Nuclear Society
Volume 29, Number 5, pp. 406~416, October 1997

An LMR Core Thermal-Hydraulics Code Based on the ENERGY Model

Won Sik Yang
Chosun University
P.O.Box 275, Kwangju, 501-600

(Received April 24, 1997)

Abstract

A computational method is developed for predicting the steady-state temperature field in an LMR core. Detailed core-wide coolant temperature profiles are efficiently calculated using the simplified energy equation mixing model[1] and the subchannel analysis method. The θ-method is employed for discretizing the energy equations in the axial direction. The interassembly coupling is achieved by interassembly gap flow. Cladding and fuel temperatures are calculated with the one-dimensional conduction model and temperature integrals of conductivities. The accuracy of the method is tested by performing several benchmark calculations for two LMR problems. The results indicate that the accuracy is comparable to the other methods based on ENERGY model. It is also shown that the implicit scheme for the axial discretization is more efficient than the explicit scheme.

1. Introductions

The thermal-hydraulics design of a liquid metal reactor (LMR) must conform to a set of design bases. Many of these relate to fuel, cladding, and sodium outlet temperatures under various conditions. For example, no fuel melting should occur at some specified overpower; the maximum allowable cladding temperature must assure fuel pin integrity; the maximum allowable sodium outlet temperature must assure a margin to boiling and structural integrity above the core. In order to ensure that these design bases are satisfied, detailed core-wide temperature calculations need to be performed. In addition, detailed temperature profiles are also required for assembly structural analysis, and sodium outlet temperatures are routinely needed for each reactor operating cycle.

For repeated detailed core-wide temperature calculations, a fast-running thermal hydraulic code is necessary. However, it requires a large amount of computer time to solve the flow equations for every channel in a core using the conventional subchannel analysis model. In order to enhance the computational efficiency, the simplified energy equation mixing model called ENERGY was developed in mid 1970s specifically for LMRs.[1-3] The simplicity of the model results from the replacement of the exact momentum coupling between channels with approximations appropriate for wire-wrapped LMR assemblies. This ENERGY model calculates the temperature distribution for forced convection problems with accuracy comparable to the detailed subchannel analysis model in a short computer time.[4-5]

Based on this ENERGY model, ENERGY[1,2] and SUPERENERGY[3] codes were developed at Massachusetts Institute of Technology (MIT) in mid 1970s. The ENERGY code performs single assembly analyses, while the SUPERENERGY code provides the

multi-assembly calculational capability. In early 1980s, the SUPERENERGY-2 code[4] was developed at Pacific Northwest Laboratory by extending the ENERGY and SUPERENERGY codes. This is a multi-assembly, steady-state subchannel analysis code for forced convection problems. More recently, the SE2-ANL code[5] was developed at Argonne National Laboratory (ANL) by modifying the SUPERENERGY-2 code. At Argonne, the SUPERENERGY-2 code was interfaced with ANL heating calculations. Reactor hot spot analysis methods as well as fuel and cladding temperature calculation models were also added to SUPERENERGY-2.

SUPERENERGY-2 and its modified version SE2-ANL have been successfully used for LMR core thermal-hydraulic design and performance analyses. However, the explicit differencing scheme employed in finite differencing of the axial convection term of the energy equation requires relatively small axial meshes to satisfy the stability criteria, and hence makes it impractical to model the axial convection due to the interassembly gap flow, which is generally small. To represent the interassembly heat transfer in the case of a small interassembly gap flow, therefore, they use a one-dimensional conduction model by assuming that the interassembly gap sodium is stagnant.[4]

The work reported here improves the numerical schemes of SUPERENERGY-2 to accommodate the axial convection due to the interassembly gap flow and to enhance the computational efficiency. Fuel and cladding temperature calculation models similar to those of SE2-ANL are also developed, and recent correlations for the flow split and mixing parameters are incorporated. The paper first describes the computational models and then formulates the numerical equations. Lastly, the results of the benchmark calculations are presented.

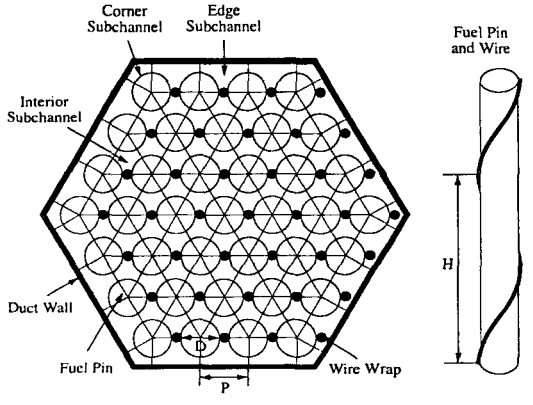

Fig. 1. Flow Subchannels in a 37-Pin Assembly

2. Computational Models

2.1 Coolant Temperature

For the thermal-hydraulic analysis of a wire-wrapped LMR rod bundle, the subchannel analysis method is commonly used. A bulk average value characterizes each of the hydrodynamic and thermal coolant conditions in every axial control volume of each subchannel. The conventional subchannel definition and key geometrical parameters for a wire-wrapped LMR assembly are illustrated in Fig. 1.

The efficiency of the ENERGY model in both computer storage and run time is due to the simplicity of its computational model where only the energy equations are solved, and the momentum and continuity equations are not directly included. The momentum coupling between coolant channels is indirectly taken into account using enhanced eddy diffusivity and the swirl velocity ratio. The derivation of the model starts by dividing the rod array of an LMR assembly into two predominant regions, the central and wall regions, instead of the entire number of subchannels and by assuming characteristic flows in each region.[1-2] The central region includes the interior subchannels, and the wall region includes the edge and corner subchannels. The flow regions and the flow directions are shown in Fig. 2.

In the central region, the flow pattern is approximated by a uniform average axial flow and an enhanced eddy diffusivity. The enhanced eddy diffusivity models the oscillatory lateral flows between sub-

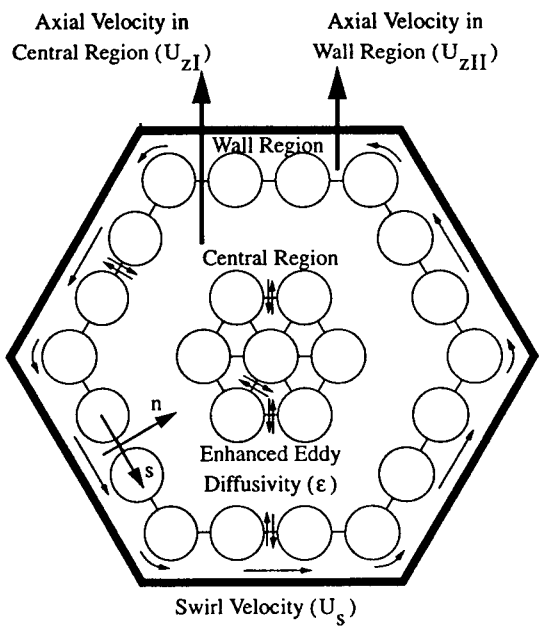

Fig. 2. Flow Fields in the Two-Region Energy Model

channels due to the presence of wire-wraps and the natural turbulence mixing. In the wall region, the velocity field is approximated by a uniform axial and a uniform circumferential component. The circumferential component represents the unidirectional cross flow along the duct wall induced by wire-wraps. The mixing between subchannels is again modeled using the enhanced eddy diffusivity as in the central region.

Energy transport equations are then derived based on these four parameters; two axial velocities in the central and wall regions (U_{zI} and U_{zII}, respectively), one circumferential velocity in the wall region (U_s), and one enhanced eddy diffusivity for heat (ε). The resulting equations for subchannels in the central and wall regions are respectively given by

$$\rho c_p U_{zI}\frac{\partial T}{\partial z} = (\rho c_p \varepsilon_I + \zeta k)\left(\frac{\partial^2 T}{\partial x^2} + \frac{\partial^2 T}{\partial y^2}\right) + Q \quad (1)$$

$$\rho c_p U_s \frac{\partial T}{\partial s} + \rho c_p U_{zII}\frac{\partial T}{\partial z} = (\rho c_p \varepsilon_n + \zeta k)\frac{\partial^2 T}{\partial n^2} + (\rho c_p \varepsilon_s + \zeta k)\frac{\partial^2 T}{\partial s^2} + Q \quad (2)$$

where T, ρ, c_p, and k represent the temperature, density, specific heat, and thermal conductivity of the coolant, respectively.[6] The terms on the left represent the axial convection and the lateral convection due to circumferential swirl flow. The first terms on the right side of the equations represent the lateral heat exchange with neighboring subchannels due to conduction and wire-wrap sweeping flows (represented by an enhanced eddy diffusivity for heat). The volumetric heat source from the fuel is given by Q. The factor $\zeta(<1)$ that multiplies the conductivity accounts for the winding (and hence lengthened) path between fuel pins followed by the sodium as energy is conducted in the direction transverse to the bulk flow.[6] The heat transfer from the duct wall in the wall region is accounted by the boundary condition.

The four parameters involved in the energy equations are obtained based on experimentally determined correlations. For a particular total flow rate, the two axial velocities in the central and wall regions are obtained from the flow split correlations determined by hydraulic diameter flow analysis and experimental data.[6-9] The flow split parameters are derived by assuming that the friction factor for each channel i can be approximated by a simple function of Reynolds number (Re_i) as

$$f_i = C_{fi} Re_i^{-m} \quad (3)$$

Using the continuity equation and the equal pressure boundary condition (i.e., the equal axial pressure drop across each subchannel of a fuel assembly), the flow velocity split is obtained as a function of subchannel equivalent diameters and the friction factor constants (C_{fi}) and exponent (m). The final flow split correlations depend on how to correlate the friction factor constants and exponent.[7-9]

The circumferential swirl velocity in the wall region is also determined using a correlation for the ratio of the transverse swirl velocity to the average axial velocity. The enhanced eddy diffusivity for heat is obtained from a correlation for the dimensionless enhanced eddy diffusivity. Both of the ratio of the trans-

verse swirl velocity to the average axial velocity and the dimensionless enhanced eddy diffusivity are correlated as functions of subchannel geometry only.[6, 8,9] The correlations for these mixing parameters are obtained by normalizing the ENERGY model to the experimental data.

2.2 Fuel Pin Temperature

A computational model for fuel and cladding temperatures is developed for metal fuels. The temperature distribution in a fuel pin is calculated using a steady-state one-dimensional radial conduction model under the assumption that the axial conduction is negligible. By dividing the cladding and fuel into concentric annuli and by integrating the conduction equation over individual annular nodes, we obtain the thermal conductivity integrals over individual nodes, which compose a system of integral equations for the temperatures at the node surfaces. This system of integral equations is converted into a system of algebraic equations by employing the correlations for thermal conductivities. The cladding thermal conductivity is assumed to be a linear function of temperature, while the fuel thermal conductivity is assumed to be a quadratic function of temperature. The fuel and cladding temperatures at each axial mesh are then determined by successively solving these algebraic equations from the outer surface of the fuel pin to the fuel center.

Integrating the one-dimensional heat conduction equation, the thermal conductivity integral over the m-th cladding node is given by[6]

$$\int_{T_c^m}^{T_c^{m+1}} k_c(T)\,dT = \frac{q''' r_f^2}{2} \ln\left(\frac{r_c^m}{r_c^{m+1}}\right) \qquad (4)$$

where r_c^m and r_c^{m+1} are the outer and the inner radius of the node m, and T_c^m and T_c^{m+1} represent the cladding temperatures at r_c^m and r_c^{m+1}, respectively. In Eq. (4), r_f and q''' are the fuel radius and the volumetric heat generation rate in the fuel. Approximating the thermal conductivity k_c by a linear function of temperature

$$k_c(T) = a + bT \qquad (5)$$

Eq. (4) is reduced to a quadratic equation for T_c^{m+1} as

$$\frac{b}{2}(T_c^{m+1})^2 + aT_c^{m+1} - \left[\frac{b}{2}(T_c^m)^2 + aT_c^m + \frac{q''' r_f^2}{2} \ln\left(\frac{r_c^m}{r_c^{m+1}}\right)\right] = 0 \qquad (6)$$

which can be easily solved using the pre-calculated T_c^m.

Similarly, the thermal conductivity integral over the m-th fuel node can be obtained as[6]

$$\int_{T_f^m}^{T_f^{m+1}} k_f(T)\,dT = \frac{q'''}{4}\left[(r_f^m)^2 - (r_f^{m+1})^2\right] \qquad (7)$$

where r_f^m and r_f^{m+1} are the outer and the inner radius of the node m, and T_f^m and T_f^{m+1} represent the fuel temperatures at r_f^m and r_f^{m+1}, respectively. This equation is reduced to a cubic equation for T_f^{m+1} as

$$\frac{\gamma}{3}(T_f^{m+1})^3 + \frac{\beta}{2}(T_f^{m+1})^2 + aT_f^{m+1} - \left[\frac{\gamma}{3}(T_f^m)^3 + \frac{\beta}{2}(T_f^m)^2 + aT_f^m + \frac{q'''}{4f(p)}\left\{(r_f^m)^2 - (r_f^{m+1})^2\right\}\right] = 0 \qquad (8)$$

by approximating the thermal conductivity k_f by a quadratic function of temperature[10] as

$$k_f(T) = f(p)(\alpha + \beta T + \gamma T^2) \qquad (9)$$

where $f(p)$ is the correction factor accounting for the irradiation effects and p is the porosity fraction of the node. The coefficients α, β, and γ are functions of weight fractions of composing isotopes in the node.

The fuel and cladding temperatures at each axial mesh are determined by successively solving Eqs. (6) and (8) from the outer surface of the fuel pin to the fuel center using the pre-calculated coolant temperature, the cladding-to-coolant heat transfer coefficient, and the fuel pin gap conductivity.

3. Numerical Formulation

The assemblies used in an LMR have two major geometrical structures. Driver, blanket, and reflector assemblies are the normal single-ducted assembly shown in Fig. 1, while the control assemblies are the double-ducted bypass assembly which consists of a central pin bundle surrounded by two hexagonal cans with a flow bypass region sandwiched between them. These two major assembly types have several variations, including different pin numbers, bundle dimensions, and duct dimensions.

In order to obtain the numerical solution for the energy equations given by Eqs. (1) and (2), each of these assemblies is radially discretized using the standard subchannel layout based on the number of pins. The interior region of the duct wall (the inner duct for the double-ducted assembly) is divided into interior, edge, and corner subchannels as shown in Fig. 1. Duct walls, bypass region, and interassembly gap are divided by extending the mesh lines of edge subchannels. The standard subchannel layout for the above two assembly types consists of seven types of subchannels shown in Fig. 3 and two types of duct wall nodes.

Heat balance equation for each axial segment of these subchannels is obtained by integrating the corresponding energy equation over the axial control volume and by approximating the temperature gradients at the lateral surfaces using a finite difference scheme. In order to couple flow channels on either side of a duct wall, a one-dimensional resistance model is employed by ignoring axial and azimuthal conductions inside a duct wall. The bypass region of the double-ducted assembly is assumed to have no circumferential swirl flow, and internodal mixing within the bypass gap is assumed to occur by conduction only. The interassembly gap flow is treated in the similar way as the bypass flow of double-ducted assembly, and the gap channels couple with the neighboring assemblies through the adjacent duct walls.

As a result of these approximations, a typical heat

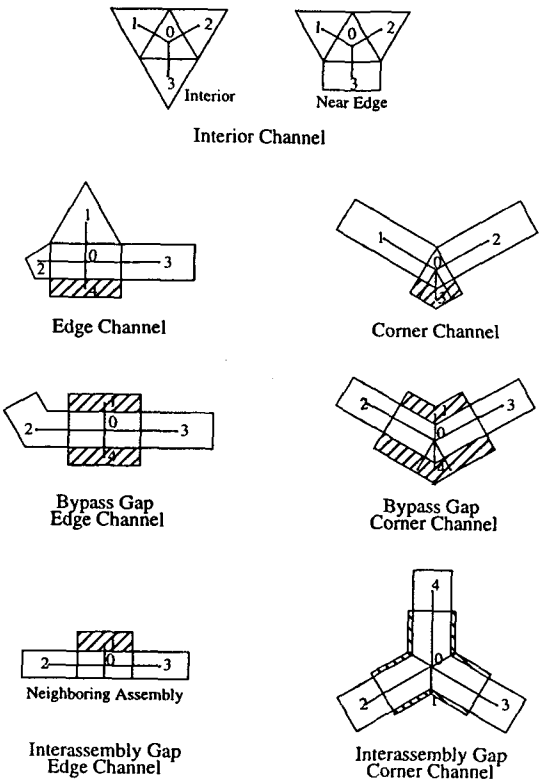

Fig. 3. LMR Assembly Subchannels and Neighboring Nodes

balance equation for a control volume is given by [11]

$$\frac{dT}{dz} = \sum_{i=1}^{I} c_i(T_i - T) + c_q q' \qquad (10)$$

where T and T_i are the coolant temperatures of the node of interest and the neighboring node i, I is the number of neighboring nodes, and q' is the linear heat generation rate in the node. The coupling coefficients c_i's depend on the mass flow rate in the node, the thermal conductivity and specific heat of sodium, and the geometrical parameters of the assembly. The coupling coefficient between subchannels also depends on the eddy diffusivity and swirl velocity as the following example between two interior subchannels :

$$c_1 = \frac{(P-D)(\zeta k + \rho c_p \varepsilon)}{m_1 c_p (P/\sqrt{3})} \qquad (11)$$

The coupling coefficient between a subchannel and a duct wall node involves the thermal resistance between them.

The finite difference approximation to Eq. (10) is obtained using the θ-method[12]. That is, Eq. (10) is integrated over the axial control volume and the integrals of temperatures are approximated by linear combinations of the top and bottom surface values. The resulting difference equation for the n-th axial mesh is as follows :

$$(1+\sum_{i=1}^{J} c_i\theta\Delta z_n)T^{n+1} - \sum_{i=1}^{J} c_i T_i^{n+1}\theta\Delta z_n \tag{12}$$
$$= T^n + \sum_{i=1}^{J} c_i(T_i^n - T^n)(1-\theta)\Delta z_n + c_q\bar{q}'_n\Delta z_n$$

where T^n and T^{n+1} are the temperatures at the bottom and top surfaces of the n-th axial mesh, $\bar{q}'_n$ is the linear heat generation rate averaged over the axial mesh, ΔZ_n is the mesh size, and θ is an arbitrary parameter in the range $0 \le \theta \le 1$. This equation is a general expression including the fully explicit and the fully implicit method ; $\theta = 0$ yields the fully explicit method, while $\theta = 1$ yields the fully implicit method. If $\theta = 1/2$, Eq.(12) becomes the Crank-Nicholson method.[12]

Including the radial boundary conditions given by heat fluxes and temperatures at the boundary, Eq. (12) can be written in the matrix notations as

$$\mathbf{A}\,\boldsymbol{T}^{n+1} = S(\boldsymbol{T}^n, \bar{\boldsymbol{q}}'_n, \boldsymbol{q}''_{bc}, \boldsymbol{T}_{bc}) \tag{13}$$

where $\boldsymbol{q}''_{bc}$ and $\boldsymbol{T}_{bc}$ are boundary heat fluxes and temperatures averaged over the axial mesh n. This equation is solved for the temperature distribution at the $n+1$st axial mesh plane, $\boldsymbol{T}^{n+1}$, using the pre-calculated $\boldsymbol{T}^n$ and given radial boundary conditions. For an implicit scheme ($\theta \neq 0$), this system of linear equations is iteratively solved. Currently, the Gauss-Seidel iterative scheme is employed for solving this equation. For a given set of inlet temperatures and radial boundary conditions, the coolant temperature distribution in the core is determined by marching in the axial direction from the bottom to the top of the core.

After coolant temperature calculation, the cladding and fuel temperatures are calculated at each axial mesh by successively solving Eqs. (6) and (8) from the outer surface of the fuel pin to the fuel center. The cubic equation given by Eq. (8) is iteratively solved using the Newton-Raphson method.

4. Numerical Results

The above computational method for predicting the steady-state temperature field in an LMR core has been implemented in a computer code, which is named SLTHEN (Steady-state LMR core Thermal-Hydraulics analysis code based on ENERGY model). Benchmark calculations have been performed for the EBR-II TED experiment problem of Reference 5 and an 840 MWt LMR model[13], and the results were compared with the reference solutions determined by SUPERENERGY-2. In order to make consistent comparisons, the same assembly flow rates and the pin power distributions used in the reference solutions were employed in these calculations. The fully explicit scheme and the fully implicit scheme were also compared for these benchmark problems.

The TED experiment problem is a seven-assembly problem consists of an experimental assembly and six neighboring assemblies as shown in Fig. 4. The experimental assembly is a 61-pin driver assembly that contains 11 dummy pins. The power and flow rate of each assembly are also shown in Fig. 4. The 840 MWt LMR problem shown in Fig. 5 has been analyzed with a one-third core model consisting of 183 assemblies. The assembly power-to-flow ratios of this problem are shown in Fig. 6. The assembly pitches of the seven-assembly problem and the 840 MWt LMR are 2.32 and 5.275 inches, respectively. The computational model for the seven-assembly problem is 55.2 inches high and divided into 1506 radial meshes, while that for the 840 MWt LMR is 120 inches high and divided into 48342 radial meshes.

The fully implicit scheme calculations were first per-

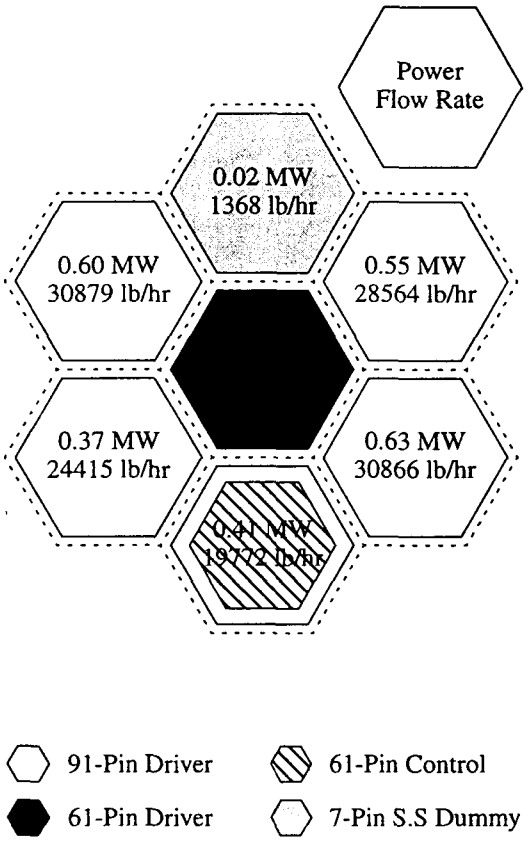

Fig. 4. Planar Layout of a Seven-Assembly Problem

formed for these problems with the interassembly gap flow of one lb/ft^2-hr used in the reference solutions, and the results were compared with the reference solutions. The axial mesh sizes of 1.016 cm (0.4 inch) and 3.81 cm (1.5 inches) were employed for the seven-assembly and the 840 MWt LMR problem, respectively. The one-dimensional conduction model of SUPERENERGY-2 was used in the reference solutions, since the flowing gap model required impractically fine axial meshes to satisfy the stability criteria. [5,13] Table 1 shows the maximum differences in the assembly outlet temperatures between SLTHEN and SUPERENERGY-2. For the driver and blanket assemblies, the results of SLTHEN agree with those of SUPERENERGY-2 to within about one °F. These results indicate that the accuracy of SLTHEN is comparable to SUPERENERGY-2.

Table 1. Maximum Differences in Assembly Outlet Temperatures (°F) Between SLTHEN and SUPERENERGY-2

		Average Temperature	Peak Temperature
Seven Assembly Problem	Drivers	0.7	1.2
	Control Rod	3.3	1.2
	Experiment Assembly	2.3	2.2
840 MWt LMR	Drivers and Blankets	0.4	0.8
	Control Rods	5.6	14.7
	Radial Reflectors and Shields	44.7	54.2

The differences in the assembly outlet temperatures between SLTHEN and SUPERENERGY-2 increase as the assembly flow rates decrease, and the maximum difference becomes greater than 50 °F for the radial reflectors and shields. These large differences for the radial reflectors and shields appear to be due to the approximations in the one-dimensional conduction model used in the reference solutions. The one-dimensional conduction model of SUPERENERGY-2 assumes that the interassembly gap sodium is stagnant, and hence it neglects the axial convection in the interassembly gap nodes. It also neglects the azimuthal conduction between interassembly gap nodes. In the driver and blanket assemblies, the flow rates are large and hence the heat is mainly removed by convection. As a result, the interassembly heat transfer is less important and the conduction model becomes a reasonable approximation to the flowing gap model. As the flow rate decreases, however, the interassembly heat transfer becomes more important and hence the errors introduced by the approximations of the conduction model becomes noticeable. For the radial reflectors and shields whose flow rates are small, the assembly outlet temperatures of the conduction model become significantly different from those of the flowing gap model. Consequently, the results of SLTHEN are expected

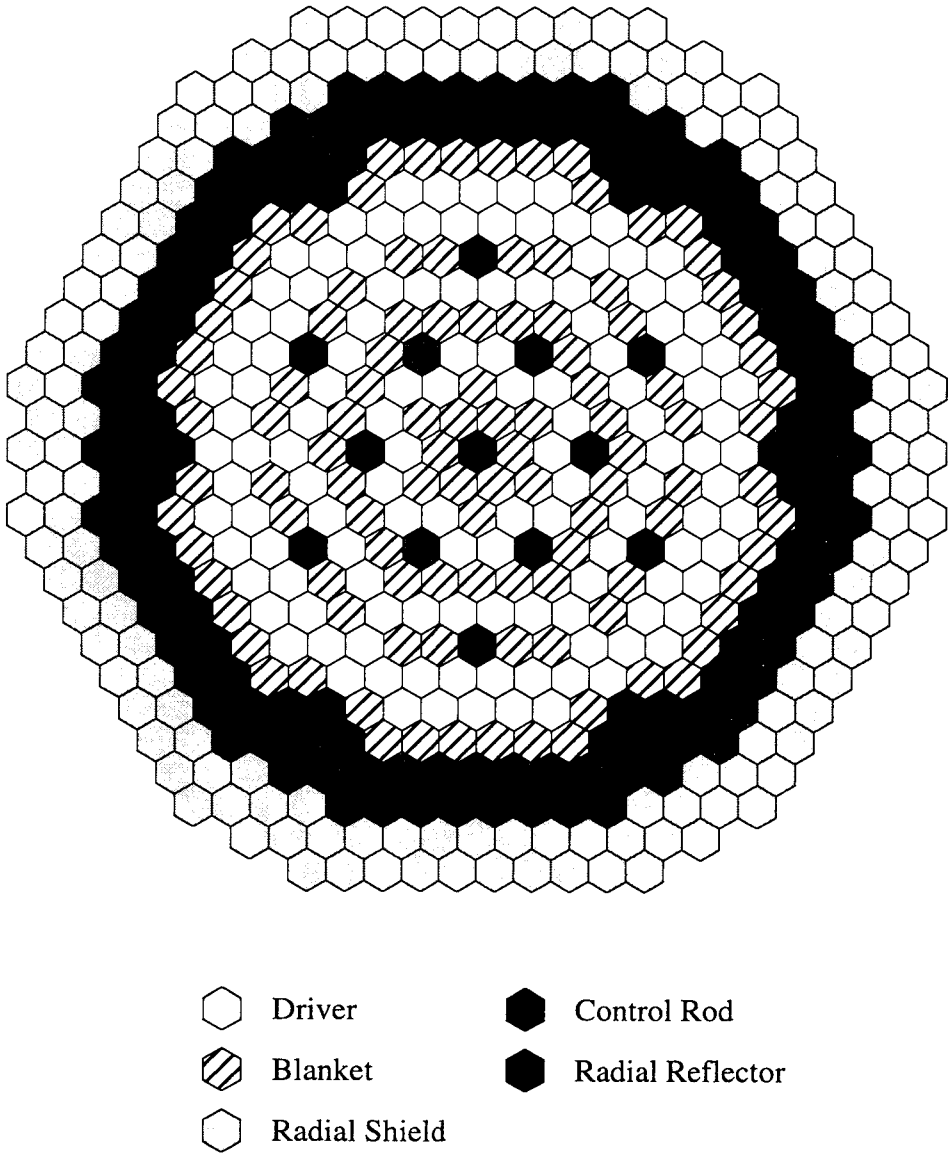

Fig. 5. Planar Layout of an 840 MWt LMR Core

to be more accurate since the approximations of the conduction model are not made in SLTHEN calculations.

The fully implicit scheme and the fully explicit scheme were also compared for these benchmark problems. For an explicit scheme calculation, the small interassembly gap flow requires a extremely fine axial mesh to satisfy the stability criteria and hence makes the calculation impractical. In order to perform the explicit scheme calculation in a reasonable computational time, the interassembly gap flow rate was arbitrarily increased from one lb/ft^2-hr to 1000 lb/ft^2-hr for the seven-assembly problem and to 10000 lb/ft^2-hr for the 840 MWt LMR model. The

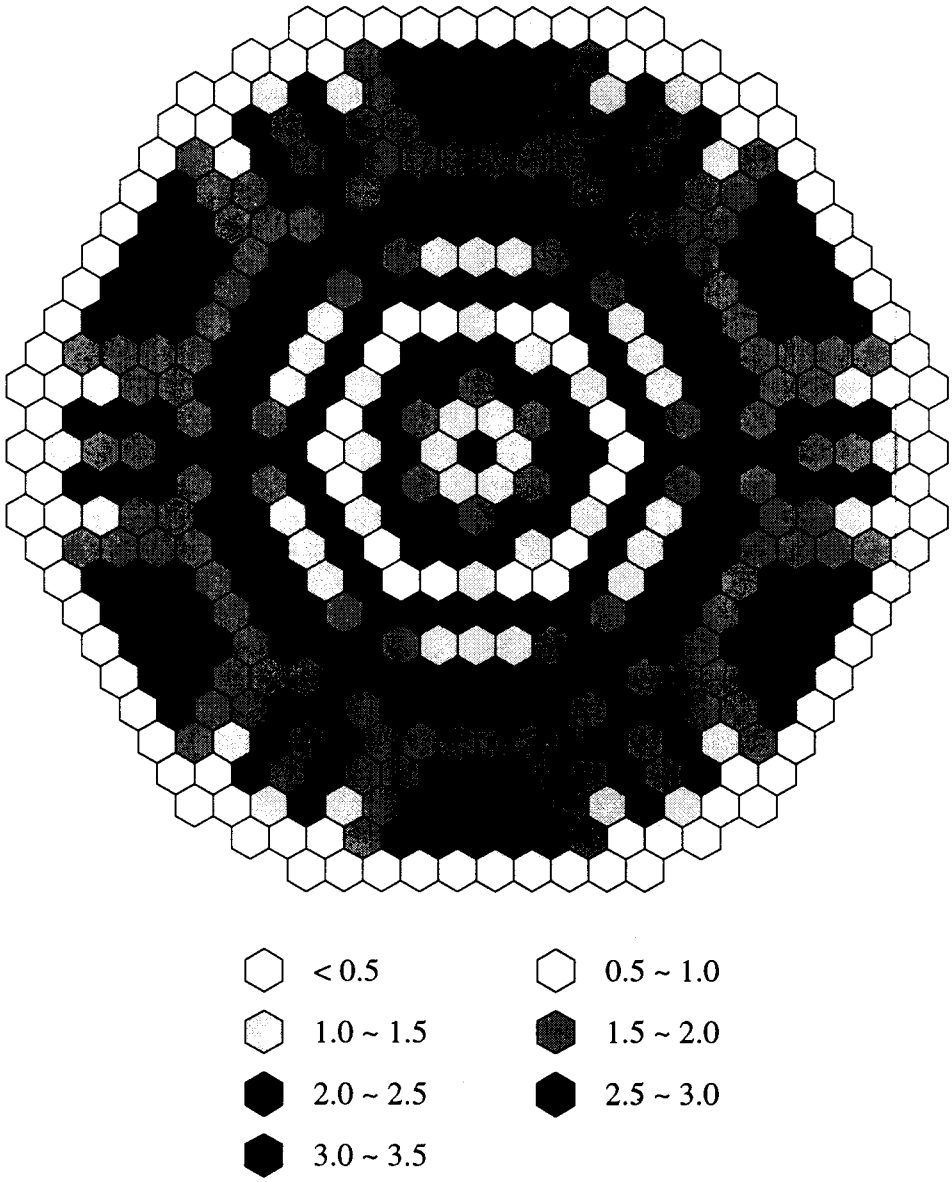

Fig. 6. Assembly Power to Flow Ratio (MJ/Kg) of an 840 MWt LMR Core

axial mesh sizes of the explicit scheme to satisfy the stability criteria was 0.0016 cm for the former and 0.0814 cm for the latter.

Table 2 shows the maximum difference in the assembly outlet temperatures between the fully explicit and the fully implicit scheme. Even though much coarser meshes are used in the implicit scheme calculations, the resulting temperatures are comparable

Table 2. Maximum Differences in Assembly Outlet Temperatures Between the Fully Implicit and the Fully Explicit Scheme

		Seven Assembly Problem	840 MWt LMR
Average Temperature	Absolute Difference(℉)	0.1	1.1
	Relative Difference(%)	0.01	0.14
Peak Temperature	Absolute Difference(℉)	1.0	1.4
	Relative Difference(%)	0.08	0.09

Table 3. Computing Times of the Fully Explicit and the Fully Implicit Scheme (SUN Sparc20)

		Seven Assembly Problem	840 MWt LMR
Number of Axial Meshes	Explicit scheme	85407	3744
	Implicit Scheme	138	80
	Ratio	618.9	46.8
Computing Time(sec)	Explicit Scheme	523	2976
	Implicit Scheme	24	1037
	Ratio	21.8	2.9

to those of the explicit scheme calculations. The computing times of these calculations are compared in Table 3. The implicit scheme is about 20 times faster than the explicit scheme for the seven-assembly problem for which the latter uses about 620 times finer axial mesh than the former. It is about three times faster for the 840 MWt LMR problem for which the explicit scheme uses about 47 times finer axial mesh. These results show that the implicit scheme is computationally more efficient than the explicit scheme and that the efficiency of the implicit scheme increases as the interassembly gap flow decreases. Considering the computer time saving relative to the reduction in the number of axial meshes, the implicit scheme calculation of the 840 MWt LMR problem takes about 1.8 times longer time than that of the seven-assembly problem. The reason is that the time for solving the system of linear equation given by Eq. (13) increases as the number of unknowns increases. Hence, the computational efficiency of the implicit scheme can be further improved by implementing an acceleration scheme or by employing other efficient solution scheme for solving the system of linear equations.

5. Conclusions

An LMR core steady-state thermal-hydraulics analysis code based on ENERGY model has been described and tested. Detailed core-wide coolant temperature profiles are efficiently calculated using the simplified energy equation mixing model and the subchannel analysis method. The θ-method is employed for discretizing the energy equations in the axial direction. The interassembly coupling is achieved by interassembly gap flow. For an implicit scheme, the system of linear equations for coolant temperatures at each axial mesh is iteratively solved using the Gauss-Seidel iterative scheme. Cladding and fuel temperatures are calculated using the one-dimensional conduction model and temperature integrals of conductivities.

To verify the code, several benchmark calculations have been performed for two LMR problems. The test results indicate that the accuracy of the code is comparable to SUPERENERGY-2 which has been validated against the detailed subchannel analysis models and measured data[4-5]. They also show that this code can be effectively used for problems of small interassembly flow to which the flowing gap model of SUPERENERGY-2 is impractical to be applied. The comparison between the fully implicit and the fully explicit scheme shows that the implicit scheme is much faster than the explicit scheme for the same accuracy. The computational efficiency of the implicit scheme can be further improved by implementing an acceleration scheme or by employing other efficient solution scheme for solving the system of linear equations for coolant temperatures

at each axial mesh.

Acknowledgement

This work was supported by the Korea Electrical Power Co. through the Electrical Engineering and Science Research Institute and the Chosun University.

References

1. E.U. Khan, W.M. Rohsenow, A.A. Sonein, and N.E. Todreas, "A Porous Body Model for Predicting Temperature Distribution in Wire-Wrapped Fuel Rod Assemblies", *Nucl. Eng. and Des.*, **35**, 1 (1975).
2. E.U. Khan, W.M. Rohsenow, A.A. Sonein, and N.E. Todreas, "A Porous Body Model for Predicting Temperature Distribution in Wire-Wrapped Rod Assemblies in Combined Forced and Free Convection," *Nucl. Eng. and Des.*, **35**, 199 (1975).
3. B. Chen and N.E. Todreas, "Prediction of Coolant Temperature Field in a Breeder Reactor Including Interassembly Heat Transfer," COO-2245-20TR, Massachusetts Institute of Technology, Cambridge (1975).
4. K.L. Basehore and N.E. Todreas, "SUPERENERGY-2 : A Multiassembly, Steady-State Computer Code for LMFBR Core Thermal-Hydraulic Analysis," PNL-3379, Pacific Northwest Laboratory, Richland, Washington (August 1982).
5. W.S. Yang and A.M. Yacout, "Assessment of the SE2-ANL Code Using EBR-II Temperature Measurements," *Proc. 7th International Meeting on Nuclear Reactor Thermal Hydraulics*, NUREG/CP-0142, Saratoga Springs, New York, September 10-15, 1995, Vol.3, p2934, US Nuclear Regulatory Commission (1995).
6. A.E. Walter and A.B. Reynolds, *Fast Breeder Reactors*, Pergamon Press, New York, New York (1981)
7. E.H. Novenstern, "Turbulent Flow Pressure Drop Model for Fuel Rod Assemblies Utilizing a Helical Wire-Wrap Spacer System," *Nucl. Eng. and Des.*, **22**, 19 (1972).
8. C. Chiu, W.M. Rohsenow, and N.E. Todreas, "Flow Split Model for LMFBR Wire Wrapped Assemblies," COO-2245-56TR, Massachusetts Institute of Technology, Cambridge (April 1978).
9. S.K. Cheng and N.E. Todreas, "Hydrodynamic Models and Correlations for Bare and Wire-Wrapped Hexagonal Rod Bundles-Bundle Friction Factors, Subchannel Friction Factors and Mixing Parameters," *Nucl. Eng. and Des.*, **92**, 227 (1986).
10. A.M. Yacout, W.S. Yang, G.L. Hofman, and Y. Orechwa, "Average Irradiation Temperature for the Analysis of In-Pile Integral Measurements," *Nuclear Technology*, **115**, 61 (1996).
11. W.S. Yang, et al., "Development of a Computer Code for LMR Core Steady-State Thermal-Hydraulics Analysis," 95-83, Electrical Engineering and Science Research Institute, Seoul, Korea (September 1996).
12. S. Nakamura, *Computational Methods in Engineering and Science*, John Wiley & Sons, Inc., New York, New York (1977).
13. R.B. Vilim, Argonne National Laboratory, personal communication (December 1992).